Optical Materials 36 (2013) 228–231

Contents lists available at ScienceDirect

Optical Materials

journal homepage: www.elsevier.com/locate/optmat

Femtosecond laser micromachined ridge waveguide lasers in Nd:YAG ceramics

Yuechen Jia [a], Javier R. Vázquez de Aldana [b], Shavkat Akhmadaliev [c], Shengqiang Zhou [c], Feng Chen [a,*]

[a] School of Physics, State Key Laboratory of Crystal Materials and Key Laboratory of Particle Physics and Particle Irradiation (MOE), Shandong University, Jinan 250100, China
[b] Laser Microprocessing Group, Universidad de Salamanca, Salamanca 37008, Spain
[c] Institute of Ion Beam Physics and Materials Research, Helmholtz-Zentrum Dresden-Rossendorf, Dresden 01314, Germany

ARTICLE INFO

Article history:
Received 5 January 2013
Received in revised form 23 June 2013
Accepted 31 August 2013
Available online 24 September 2013

Keywords:
Optical waveguides
Nd:YAG ceramic
Femtosecond laser micromachining

ABSTRACT

We report on the fabrication of ridge waveguides in Nd:YAG ceramic by using femtosecond laser micromachining of the surface of a He ion implanted planar waveguide. Under optical pump of 808 nm light, continuous wave waveguide lasers have been realized at 1.06 μm at room temperature in the Nd:YAG ceramic ridge waveguide system, reaching a maximum output power of 46 mW. The lasing threshold of ~64.9 mW and the slope efficiency of 42.5% are obtained for the ridge waveguide system, which shows superior lasing performance to the Nd:YAG ceramic planar waveguide.

1. Introduction

As the basic elements in integrated photonics, optical waveguides with diverse configurations can confine the light propagation within small volumes owing to the much compact geometry, reaching higher optical intensities, in which, consequently, a number of bulk-related performances could be substantially improved [1]. Laser oscillations with reduced lasing thresholds could be realized in waveguide-based structures due to the in-cavity dense of the active volumes, possessing comparable efficiencies with respect to bulk lasers [2]. In practice, two-dimensionally (2D) confined waveguide structures (typically channel or ridge configurations) allow for more compact geometries and stronger spatial confinement of light fields, exhibiting superior guiding performance with respect to the one-dimensional (or planar) counterparts, and are possible to construct more compact devices which can be efficiently connected to optical fibers for construction of integrated photonic systems. Moreover, compared with planar and channel waveguides, the ridge waveguide structures usually possess much stronger lateral confinement of the light fields due to the higher refractive index contrast of the cladding and waveguide in the transverse dimension in ridge cases (the cladding is air with index of 1), which suggests a reduction of bending losses and component sizes of the photonic devices [3,4]. Particularly, the surface optical circuits (such as surface ridge guiding configurations) are especially interesting for biological applications, and they can be used as fast and sensitive bio-sensors when appropriately functionalized.

Being regarded as the next-generation highly efficient gain media for solid state laser systems, polycrystalline neodymium doped yttrium aluminum garnet ($Nd:Y_3Al_5O_{12}$ or Nd:YAG) ceramics have recently obtained much attention owing to their superior lasing and fluorescence properties [5]. Indeed, compared to their single crystalline partners, transparent Nd:YAG ceramics have demonstrated several intriguing advantages, such as better laser performance at the near-infrared bands, possibilities for realizing large-size multilayers for multipurpose laser devices, and superior spectroscopic properties [5–7]. Hence, the combination of waveguide technology with excellent properties of Nd:YAG ceramics is most likely one effective approach for constructing a high-power integrated lasers with a stable output. Even though some conventional chemical techniques (such as metal ion diffusion and ion exchange) that have been widely used for waveguide construction in diverse materials [8] are not suitable for Nd:YAG ceramics owing to their stable physical, chemical, and thermal properties. As of yet, the Nd:YAG ceramic planar and channel waveguides have been fabricated by utilizing several "physical" techniques, including ion implantation/irradiation [9] and femtosecond (fs) laser inscription [10–12]. Ion implantation, as one of the most successful methods for controlled material modifications at the micrometric scale, has been widely used to produce waveguides in versatile optical substrates, exhibiting unique capabilities to diverse materials. As a physical method, in principle, it does not rely on the chemical properties of the target materials [9,13–18]. Fs-laser inscription is a powerful and feasible way to fabricate channel waveguide

* Corresponding author. Tel.: +86 531 88363007; fax: +86 531 88363350.
E-mail address: drfchen@sdu.edu.cn (F. Chen).

0925-3467/$ - see front matter © 2013 Elsevier B.V. All rights reserved.
http://dx.doi.org/10.1016/j.optmat.2013.08.031

configurations and it has become increasingly attractive in recent years owing to the various practical applications in microstructuring of multiple materials [10–12,19–25]. In addition, with more energy of single pulses, the fs-laser ablation technique has been successfully applied to fabricate ridge waveguide structures by removing selected surface parts of the ion implanted planar waveguides of $LiNbO_3$ [26], β-BaB_2O_4 [27] and TiO_2 [28] crystals. Particularly, we have recently fabricated ridge waveguides in Nd:GGG [28], Nd:YAG [30] and Nd:GdCOB [31] single crystals through this solution, and found that the ridge waveguide systems have exhibited enhanced lasing or nonlinear optical performances with respect to planar structures. In addition, compared with the method of diamond blade dicing we used to fabricate surface ridge guiding structures in recent work [32], the fs-laser ablation technique is more convenient, swift and affordable. In this work, we report on the manufacture of Nd:YAG ceramic ridge waveguide by using the fs ablating of the surface of He^+ ion implanted planar waveguide, and the realization of continuous wave (cw) ridge waveguide laser oscillations at 1.06 μm.

2. Experiments in details

The Nd:YAG ceramic (doped by 1% at Nd^{3+} ions) used in this work was cut with the dimensions of $7 \times 7 \times 2$ mm^3 and optically polished. In the first place, a planar waveguide layer was prepared on one surface (7×7 mm^2) of the sample by using He^+ ions implantation at energy of 2.5 MeV and fluence of 1×10^{16} ions/cm^2. The implantation process was performed by using the 3 MV tandem accelerator at Helmholtz–Zentrum Dresden–Rossendorf, Germany. In this way, a planar waveguide layer was fabricated on top of the Nd:YAG ceramic surface. Afterwards, an amplified Ti:Sapphire laser system (Spitfire, Spectra Physics) generating nearly transform-limited pulses with a temporal duration of 120 fs and a central wavelength of 796 nm and with a repetition rate of 1 kHz (1 mJ maximum pulse energy), was used to micro-machine ridge structures on top of the implanted planar waveguide surface. The fs laser beam was focused by a 20× microscope objective (N.A. = 0.4), and the sample was located at a 3D x–y–z motorized stage with a spatial resolution of 0.2 μm. The linear focus of the convex was located on the surface of the planar waveguide and the pulse energy was set to 4.2 μJ (peak fluence ~100 J/cm^2). The sample was scanned at a translation velocity of 50 μm/s, as a compromise between having a moderate processing time and obtaining the crater depth enough to cut through the planar waveguide layer. Then, pairs of grooves were fabricated with lateral separation of 70 μm to have a restrictive effect laterally. And combined with vertical confinement of ion implanted planar waveguide, the ridge waveguide was fabricated in Nd:YAG ceramic. Fig. 1(a) illustrates the microscope image of the cross section of the ridge waveguide. For comparison, about 1/3 of the surface layer was not microstructured, preserving the planar waveguide geometry.

The m-line technique was utilized to measure the surface refractive index of the sample and surface waveguide mode via a prism coupler (Model 2010, Metricon). An end-face coupling arrangement was used to experimentally estimate the propagation losses for the Nd:YAG ceramic ridge and planar waveguides, which are measured to be 4.8 dB/cm and 3.4 dB/cm at 632.8 nm by using the back-reflection method [33]. The higher attenuation for ridge waveguide is very likely due to the non-perfect side-walls fabricated by fs laser ablation. In order to investigate the roughness of the side-walls, we used scanning electron microscopy (SEM) to obtain the surface topographic image of the ridge waveguide (see Fig. 1(b)). As we can see, the roughness of the sidewall is estimated to be ~2.0 μm. When compared with the previous work on ridge waveguides produced by using diamond blade dicing method in [32], we found that the propagation loss of ridge waveguide in this work is higher. This may partly be due to the higher attenuation of He ion implanted planar waveguide used in this work (in diamond blade diced case, the propagation loss of carbon irradiated planar waveguide was around ~1.0 dB/cm) as well as the non-perfect side-walls of the fs laser ablated grooves (in diamond blade diced case, the side-walls are considerably smooth).

The waveguide laser operation experiment was performed by utilizing an end pumping system. A polarized light beam at a wavelength of 808 nm was generated from a tunable cw Ti:Sapphire laser (Coherent MBR 110) at room temperature. We used a spherical convex less with focal length of 25 mm to couple the laser beam into the waveguides. In order to form the Fabry–Perot lasing resonate cavity, the input and output end faces of the waveguides were adhered with an input mirror (with the transmittance of 98% at 808 nm and the reflectivity >99% at ~1064 nm, respectively) and an output mirror (with the reflectivity >99% at 808 nm and the transmittance of approximately 60% at ~1064 nm, respectively). A 20× microscope objective lens (N.A. = 0.4) and an infrared CCD were used to collect and image the generated waveguide lasers. The emission spectra of the laser beam from the waveguide were analyzed by a spectrometer with resolution of 0.2 nm.

3. Results and discussion

We used the reflectivity calculation method (RCM) [34] to reconstruct the refractive index profile (Fig. 2) of the He^+ ions implanted waveguide based on the measured dark-mode spectra. As we can see, the 2.5 MeV He^+ implantation induced a positive index change of 0.04% in the near-surface region and an optical barrier with reduced refractive index of 0.5% at the end of incident ion track (5.5 μm beneath the surface of the sample). And the energy deposition process of 2.5 MeV He^+ ions when implanted onto

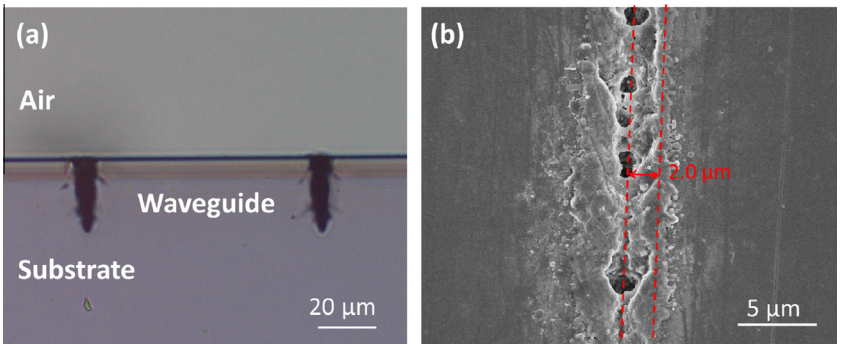

Fig. 1. The cross sectional microscope image of the end face of the Nd:YAG ceramic ridge waveguide and (b) topographic SEM image of the ridge waveguide surface.

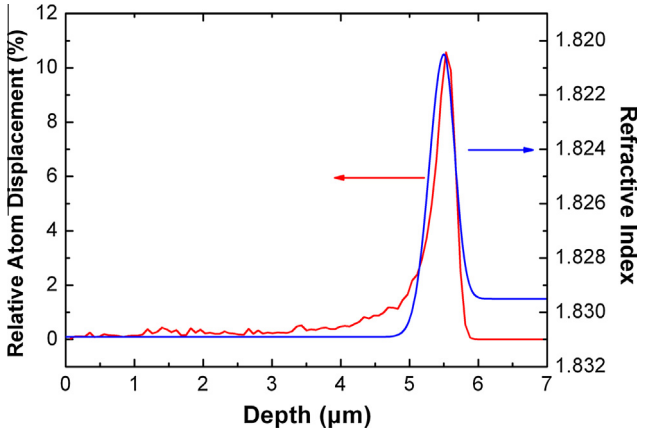

Fig. 2. The refractive index and relative atom displacement of the original profiles in Nd:YAG ceramic induced by 2.5 MeV He^+ implantation at the fluence of 1×10^{16} ions/cm^2.

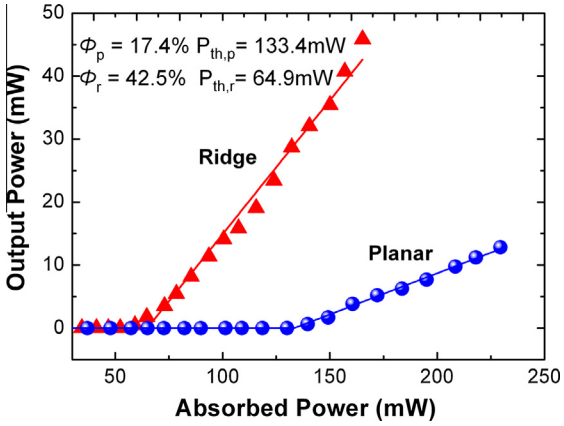

Fig. 4. The cw waveguide laser output powers at 1064 nm as a function of the absorbed power at 808 nm. The circular and triangular symbols stand for the data of the planar and ridge waveguides, respectively. The solid lines represent the linear fit of the experimental data.

Nd:YAG ceramic was simulated with stopping and range of ions in matter (SRIM) 2010 code [35]. The resulting relative atom displacement distribution of the original lattice induced by He^+ ions implantation is shown in Fig. 2. As indicated, the values of relative atom displacement are obtained within the range of 0–6 μm, peaking above 10% at approximately 5.5 μm, which is in good agreement with optical barrier location. In addition, this distribution also considerably coincides with the refractive index profiles, suggesting that the lattice damage induced by nuclear collisions is the main reason for the waveguides formation.

Fig. 3 illustrates the room temperature laser emission spectra from 2.5 MeV He^+ implanted Nd:YAG ceramic ridge and planar waveguides when the absorbed power is above the lasing threshold. The emission line centered at 1064 nm with a FWHM of ~0.5 nm, clearly denoting laser oscillation line that corresponds to main fluorescence of $^4F_{3/2} \rightarrow {}^4I_{11/2}$ transition of Nd^{3+} ions. The insets depict the near-field light intensity profiles of the ridge and planar waveguide laser modes.

Fig. 4 shows the output laser powers (at wavelength of 1064 nm) as a function of the 808 nm absorbed power generated in the Nd:YAG ceramic planar and ridge waveguides at room temperature. From the linear fit of the experimental data, we have determined that the lasing thresholds for the 1064 nm oscillations are $P_{th,p} = 133.4$ mW and $P_{th,r} = 64.9$ mW for Nd:YAG planar and ridge waveguides, respectively. And the slope efficiencies are $\Phi_p = 17.4\%$ and $\Phi_r = 42.5\%$, respectively. As the absorbed pump power increases, the output laser power of these two waveguides climbed to maxima at $P_{max,p} = 13$ mW and $P_{max,r} = 46$ mW at absorbed pump powers of 230 and 165 mW, corresponding to optical conversion efficiencies of 6% and 28%, respectively. In conclude, the ridge waveguide system possesses a superior performance with reduced lasing threshold, higher slope efficiency and higher output laser power with respect to planar waveguide, although the propagation loss of ridge waveguide is higher. In addition, compared with the other fs-laser micromachined ridge waveguides (i.e. Nd:GGG [28] and Nd:YAG [29] crystal ridge waveguides) we studied recently, the Nd:YAG ceramic ridge waveguide exhibits an comparable excellent laser performance with larger maximum output laser power (for Nd:GGG and Nd:YAG ones, the results are 25.6 and 21 mW, respectively) and higher slope efficiency (for cases with Nd:GGG and Nd:YAG crystal, those are 41.8% and 35%, respectively). Though the lasing threshold of the Nd:YAG ceramic ridge waveguide laser is higher than that of Nd:YAG crystal one (which is 39 mW), it is still lower than that of Nd:GGG case (with a lasing threshold of 71.6 mW). Thus, all the results above indicate that the Nd:YAG ceramic ridge waveguide produced by fs-laser micromachining of planar waveguide layer could be a promising candidate for compact light sources.

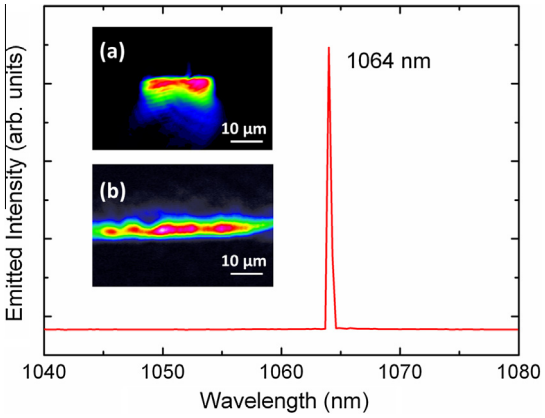

Fig. 3. Laser emission spectrum from the ridge and planar Nd:YAG ceramic waveguides. The insets show the measured near-field intensity distribution of the (a) ridge and (b) planar waveguide laser modes.

4. Conclusion

We have reported on the fabrication of optical ridge waveguide in Nd:YAG ceramics, using fs laser ablation of the surface of He^+ ion implanted planar waveguide. The cw waveguide laser at 1064 nm was realized with a pump threshold of 64.9 mW and a slope efficiency of 42.5%. For comparison, the fs laser micromachined Nd:YAG ceramic ridge waveguide shows a more excellent laser performance than planar waveguide under the same condition. This work has shown the fs laser ablation technique combined with ion implantation is an efficient method to realize Nd:YAG ceramic ridge waveguide laser sources.

Acknowledgements

The work is supported by the National Natural Science Foundation of China (No. 10925524), the Spanish Ministerio de Ciencia e Innovación (MICINN) through Consolider Program SAUUL CSD2007-00013, Project FIS2009-09522 and Junta de Castilla y León (Project SA086A12-2). S.Z. acknowledges the funding by the Helmholtz-Gemeinschaft Deutscher Forschungszentren (HGF-VH-

NG-713). Support from the Centro de Láseres Pulsados (CLPU) is also acknowledged.

References

[1] E.J. Murphy, Integrated Optical Circuits and Components: Design and Applications, Marcel Dekker, New York, 1999.
[2] C. Grivas, Prog. Quantum Electron. 35 (2011) 159–239.
[3] F. Chen, Crit. Rev. Solid State Mater. Sci. 33 (2008) 165–182.
[4] G. Lifante, Integrated Photonics: Fundamentals, Wiley, Atrium, 2008.
[5] A. Ikesue, Y.L. Aung, T. Taira, G.L. Messing, Annu. Rev. Mater. Res. 36 (2006) 397–429.
[6] A.A. Kaminskii, Laser Photonics Rev. 1 (2007) 93–177.
[7] C. Jacinto, A. Benayas, T. Catunda, J. García-Solé, A.A. Kaminskii, D. Jaque, J. Chem. Phys. 129 (2008) 104705.
[8] H. Suche, R. Wessel, S. Westenhöer, W. Sohler, S. Bosso, C. Carmannini, R. Corsini, Opt. Lett. 20 (1995) 596–598.
[9] Y. Tan, C. Zhang, F. Chen, F.Q. Liu, D. Jaque, Q.M. Lu, Appl. Phys. B 103 (2011) 837–840.
[10] G.A. Torchia, P.F. Meilán, A. Rodenas, D. Jaque, C. Mendez, L. Roso, Opt. Express 15 (2007) 13266.
[11] G.A. Torchia, A. Rodenas, A. Benayas, E. Cantelar, L. Roso, D. Jaque, Appl. Phys. Lett. 92 (2008) 111103.
[12] H.L. Liu, Y.C. Jia, J.R. Vázquez de Aldana, D. Jaque, F. Chen, Opt. Express 20 (2012) 18620–18629.
[13] P.D. Townsend, P.J. Chandler, L. Zhang, Optical Effects of Ion Implantation, Cambridge Univ. Press, Cambridge, 1994.
[14] A. García-Navarro, J. Olivares, G. García, F. Agulló-López, S. García-Blanco, C. Merchant, J.S. Aitchison, Nucl. Instrum. Methods Phys. Res. B 249 (2006) 177–180.
[15] G.B. Montanari, P. De Nicola, S. Sugliani, A. Menin, A. Parini, A. Nubile, G. Bellanca, M. Chiarini, M. Bianconi, G.G. Bentini, Opt. Express 20 (2012) 4444–4453.
[16] M. Domenech, G.V. Vázquez, E. Flores-Romero, E. Cantelar, G. Lifante, Appl. Phys. Lett. 86 (2005) 151108.
[17] J. Olivares, G. García, A. García-Navarro, F. Agulló-López, O. Caballero, A. García-Cabañes, Appl. Phys. Lett. 86 (2005) 183501.
[18] A.A. Bettiol, S.V. Rao, E.J. Teo, J.A. van Kan, F. Watt, Appl. Phys. Lett. 88 (2006) 171106.
[19] K.M. Davis, K. Miura, N. Sugimoto, K. Hirao, Opt. Lett. 21 (1996) 1729–1731.
[20] R.R. Gattass, E. Mazur, Nat. Photonics 2 (2008) 219–225.
[21] M. Ams, G.D. Marshall, P. Dekker, J. Piper, M. Withford, Laser Photonic. Rev. 3 (2009) 535–544.
[22] A. Zoubir, C. Lopez, M. Richardson, K. Richardson, Opt. Lett. 29 (2004) 1840–1842.
[23] V. Apostolopoulos, L. Laversenne, T. Colomb, C. Depeursinge, R.P. Salathe, M. Pollnau, R. Osellame, G. Cerullo, P. Laporta, Appl. Phys. Lett. 85 (2004) 1122–1124.
[24] A. Rodenas, A.K. Kar, Opt. Express 19 (2011) 17820–17833.
[25] T. Calmano, A.G. Paschke, J. Siebenmorgen, S.T. Fredrich-Thornton, H. Yagi, K. Petermann, G. Huber, Appl. Phys. B 103 (2011) 1–4.
[26] F. Chen, J. Appl. Phys. 106 (2009) 081101.
[27] R. Degl'Innocenti, S. Reidt, A. Guarino, D. Rezzonico, G. Poberaj, P. Günter, J. Appl. Phys. 100 (2006) 113121.
[28] Z.F. Bi, L. Wang, X.H. Liu, S.M. Zhang, M.M. Dong, Q.Z. Zhao, X.L. Wu, K.M. Wang, Opt. Express 20 (2012) 6712–6719.
[29] Y.C. Jia, N.N. Dong, F. Chen, J.R. Vázquez de Aldana, Sh. Akhmadaliev, S.Q. Zhou, Opt. Express 20 (2012) 9763–9768.
[30] Y.C. Jia, N.N. Dong, F. Chen, J.R. Vázquez de Aldana, Sh. Akhmadaliev, S.Q. Zhou, Opt. Mater. Express 2 (2012) 657–662.
[31] Y.C. Jia, F. Chen, J.R. Vázquez de Aldana, Sh. Akhmadaliev, S.Q. Zhou, Opt. Mater. 34 (2012) 1913–1916.
[32] Y.C. Jia, C.E. Rüter, S. Akhmadaliev, S.Q. Zhou, F. Chen, D. Kip, Opt. Mater. Express 3 (2013) 433–438.
[33] R. Ramponi, R. Osellame, M. Marangoni, Rev. Sci. Instrum. 73 (2002) 1117–1120.
[34] P.J. Chandler, F.L. Lama, Opt. Acta 33 (1986) 127–143.
[35] J.F. Ziegler, computer code, SRIM <http://www.srim.org>.